

Full Duplex Holographic MIMO for Near-Field Integrated Sensing and Communications

Ioannis Gavras*, Md Atiqul Islam[†], Besma Smida[‡], and George C. Alexandropoulos*

*Department of Informatics and Telecommunications, National and Kapodistrian University of Athens, Greece

[†]Qualcomm Technologies, Inc., Santa Clara, CA, USA

[‡]Department of Electrical and Computer Engineering, University of Illinois at Chicago, USA

emails: {sdi1900029, alexandg}@di.uoa.gr, mdatiqul@qti.qualcomm.com, smida@uic.edu

Abstract—This paper presents an in-band Full Duplex (FD) integrated sensing and communications system comprising a holographic Multiple-Input Multiple-Output (MIMO) base station, which is capable to simultaneously communicate with multiple users in the downlink direction, while sensing targets being randomly distributed within its coverage area. Considering near-field wireless operation at THz frequencies, the FD node adopts dynamic metasurface antenna panels for both transmission and reception, which consist of massive numbers of sub-wavelength-spaced metamaterials, enabling reduced cost and power consumption analog precoding and combining. We devise an optimization framework for the FD node’s reconfigurable parameters with the dual objective of maximizing the targets’ parameters estimation accuracy and the downlink communication performance. Our simulation results verify the integrated sensing and communications capability of the proposed FD holographic MIMO system, showcasing the interplays among its various design parameters.

Index Terms—Full duplex, holographic MIMO, integrated communications and sensing, near-field, THz, metasurfaces.

I. INTRODUCTION

The combination of sensing and communication signaling operations under the same system infrastructure is recently gaining remarkable ground as an efficient means for improving spectral and energy efficiencies in 6th Generation (6G) networks [1], [2]. This notion of Integrated Sensing and Communications (ISAC) is lately being investigated in the framework of in-band Full Duplex (FD) Multiple-Input Multiple-Output (MIMO) radios, which enable simultaneous DownLink (DL) transmission and uplink reception (of data or control signals) within the entire frequency band [3]–[5].

The main challenge for FD MIMO ISAC systems is the Self-Interference (SI) signal induced from the multi-antenna Transmitter (TX) of the FD node to its multi-antenna Receiver (RX), which increases with the number of TX antenna elements. State-of-the-art solutions include combination of propagation domain isolation, analog domain suppression, digital SI cancellation techniques, and recently, hybrid analog and digital BeamForming (BF), which has been shown to perform efficiently in FD massive MIMO systems operating in millimeter-wave frequencies [6], [7]. Single-antenna FD systems realizing joint radar communication and sensing were considered in [8], [9], while FD ISAC operations with millimeter-wave massive MIMO systems were designed in [10]–[12], showcasing the efficacy of FD systems for simultaneous data communication and target tracking. However, to the best of the authors’

knowledge, FD MIMO ISAC operating in the THz frequency band and in the near-field regime has not yet been reported.

In this paper, we present a novel FD holographic MIMO system, which is realized via the efficiently scalable technology of Dynamic Metasurface Antennas (DMAs) [13] at both its TX and RX ends. Those arrays of metamaterials are designed to enable simultaneous multi-user DL data communication and 3D direction of arrival as well as range estimation of multiple targets lying in the vicinity of the proposed FD-enabled ISAC system. Considering wireless operation in the THz frequency band and in the near-field regime, we assume that the targets reflect the DL signals back to the FD holographic MIMO system, enabling their spatial parameters’ tracking. By modeling signal propagation over the metamaterial-based microstrips comprising each DMA as well as their tunable frequency responses, we present a novel optimization framework for the joint desing of the TX/RX DMAs’ analog BF matrices, the TX digital BF matrix, and the digital SI cancellation matrix, having a dual objective that includes the DL rate and the accuracy of the target parameters’ estimation. An extensive waveform simulation at sub-THz frequencies verifies the performance of the proposed FD holographic MIMO ISAC system.

Notations: Vectors and matrices are denoted by boldface lowercase and boldface capital letters, respectively. The transpose, Hermitian transpose, and the inverse of \mathbf{A} are denoted by \mathbf{A}^T , \mathbf{A}^H , and \mathbf{A}^{-1} , respectively, while \mathbf{I}_n and $\mathbf{0}_n$ ($n \geq 2$) are the $n \times n$ identity and zeros’ matrices, respectively. $[\mathbf{A}]_{i,j}$ is the (i, j) -th element of \mathbf{A} , $\|\mathbf{A}\|$ returns \mathbf{A} ’s Euclidean norm, $|a|$ is the amplitude of a complex scalar a , \mathbb{C} is the complex number set, and j is the imaginary unit. $\mathbb{E}\{\cdot\}$ is the expectation operator and $\mathbf{x} \sim \mathcal{CN}(\mathbf{a}, \mathbf{A})$ indicates a complex Gaussian random vector with mean \mathbf{a} and covariance matrix \mathbf{A} .

II. SYSTEM AND SIGNAL MODELS

We consider an FD-enabled ISAC system comprising an FD holographic MIMO node equipped with TX and RX DMAs [13], which wishes to communicate in the DL direction with U multi-antenna User Equipment (UEs), while simultaneously being capable to sense $K \geq U$ radar targets lying in its vicinity. It is assumed that the U served UEs are fixed, belonging to the K sensed targets. DMAs can efficiently realize holographic MIMO transceivers [14], facilitating packaging larger number of sub-wavelength-spaced metamaterials

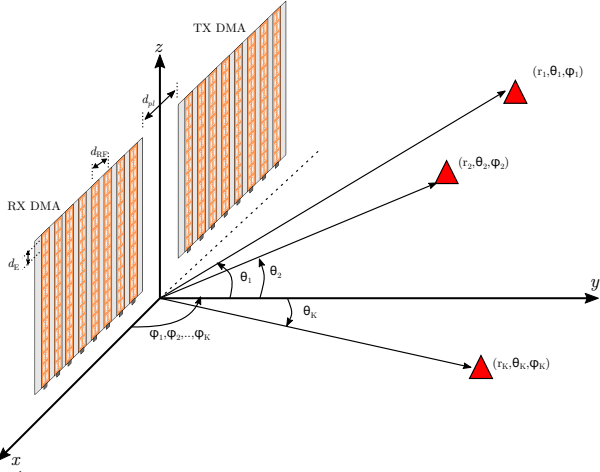


Fig. 1: The proposed FD holographic MIMO system enabling ISAC. d_{RF} is the distance between adjacent microstrips in each DMA, d_E is the inter-element distance within each microstrip, and $d_{\text{pl}} = 2d_E$ is the horizontal separation between the TX and RX DMAs.

in given apertures. They consist of single-RF-fed microstrips, where the transmitted/received signals are phase-controlled via metamaterials of dynamically tunable frequency responses, thus, implementing analog BF. As shown in Fig. 1, the TX and RX DMA panels of the FD MIMO node are placed in the xz -plane centered at the origin. N_{RF} microstrips with N_E metamaterials of inter-element spacing of d_E are assumed in both TX and RX DMAs, each connected to a respective Radio Frequency (RF) chain. Hence, both the TX and RX have $N \triangleq N_{\text{RF}}N_E$ metamaterials. Finally, all U UEs are equipped with L -element all-digital Uniform Linear Arrays (ULA), which are placed for simplicity on the z -axis.

We define the $N \times N$ diagonal matrices \mathbf{P}_{TX} and \mathbf{P}_{RX} , whose elements model the signal propagation inside the microstrips at the TX and RX DMAs, respectively. The former is defined $\forall i = 1, \dots, N_{\text{RF}}$ and $\forall n = 1, \dots, N_E$ by [15]:

$$[\mathbf{P}_{\text{TX}}]_{((i-1)N_E+n, (i-1)N_E+n)} \triangleq \exp(-\rho_{i,n}(\alpha_i + j\beta_i)), \quad (1)$$

where α_i is the waveguide attenuation coefficient, β_i is the wavenumber, and $\rho_{i,n}$ denotes the location of the n th element in the i th microstrip. Similar is the definition for \mathbf{P}_{RX} . Let $w_{i,n}^{\text{TX}}$ denote the tunable response (i.e., analog weight) of each n th metamaterial of each i th microstrip, which is assumed to follow a Lorentzian-constrained phase model and belong to the phase profile codebook \mathcal{W} :

$$w_{i,n}^{\text{TX}} \in \mathcal{W} \triangleq \left\{ \frac{j + e^{j\phi}}{2} \mid \phi \in \left[-\frac{\pi}{2}, \frac{\pi}{2} \right] \right\}. \quad (2)$$

The analog TX BF matrix $\mathbf{W}_{\text{TX}} \in \mathbb{C}^{N \times N_{\text{RF}}}$ is given by:

$$[\mathbf{W}_{\text{TX}}]_{((i-1)N_E+n, j)} = \begin{cases} w_{i,n}^{\text{TX}}, & i = j, \\ 0, & i \neq j. \end{cases} \quad (3)$$

Similarly, we define the weights $w_{i,n}^{\text{RX}} \in \mathcal{W} \forall i, n$, from which the analog RX BF matrix $\mathbf{W}_{\text{RX}} \in \mathbb{C}^{N \times N_{\text{RF}}}$ is formulated.

The DMA-based TX of the proposed FD holographic MIMO system possesses the symbol vector $\mathbf{s}_u \in \mathbb{C}^{L \times 1}$ for

each u th UE which is first precoded via the digital BF matrix $\mathbf{V}_u \in \mathbb{C}^{N_{\text{RF}} \times L}$. Before transmission in the DL, the digitally precoded symbols are analog processed via the weights of the TX DMA, resulting in the N -element transmitted signal $\mathbf{x} \triangleq \mathbf{P}_{\text{TX}}\mathbf{W}_{\text{TX}}\mathbf{V}_u\mathbf{s}_u$ where $\mathbf{V} \triangleq [\mathbf{V}_1, \dots, \mathbf{V}_U] \in \mathbb{C}^{N_{\text{RF}} \times UL}$ and $\mathbf{s} \triangleq [\mathbf{s}_1^T, \dots, \mathbf{s}_U^T]^T \in \mathbb{C}^{UL \times 1}$. We finally assume this signal is power limited such that $\mathbb{E}\{\|\mathbf{P}_{\text{TX}}\mathbf{W}_{\text{TX}}\mathbf{V}_u\mathbf{s}_u\|^2\} \leq P_{\text{max}}$, where P_{max} being the maximum transmission power.

A. Near-Field Channel Model

We consider wireless operation in the THz frequency band, which takes place in a near-field signal propagation environment, as shown in Fig. 1. Each $L \times N$ complex-valued DL channel (i.e., for each u th UE) is modeled as follows:

$$[\mathbf{H}_{\text{DL},u}]_{(\ell, (i-1)N_E+n)} \triangleq \alpha_{u,\ell,i,n} \exp\left(\frac{j2\pi}{\lambda} r_{u,\ell,i,n}\right), \quad (4)$$

where $r_{u,\ell,i,n}$ represents the distance between the ℓ th antenna ($\ell = 1, \dots, L$) of each u th UE and the n th meta-element of each i th TX DMA's RF chain. In addition, $\alpha_{u,\ell,i,n}$ defines the respective attenuation factor with molecular absorption coefficient κ_{abs} at THz, which is defined as:

$$\alpha_{u,\ell,i,n} \triangleq \sqrt{F(\theta_{u,\ell,i,n})} \frac{\lambda}{4\pi r_{u,\ell,i,n}} \exp\left(-\frac{\kappa_{\text{abs}} r_{u,\ell,i,n}}{2}\right) \quad (5)$$

with λ being the wavelength and $F(\cdot)$ is each metamaterial's radiation profile, modeled for an elevation angle θ as follows:

$$F(\theta) = \begin{cases} 2(b+1) \cos^b(\theta), & \text{if } \theta \in \left[-\frac{\pi}{2}, \frac{\pi}{2}\right], \\ 0, & \text{otherwise.} \end{cases} \quad (6)$$

In the latter expression, b determines the boresight antenna gain which depends on the specific DMA technology.

As depicted in Fig. 1, we consider K targets with spherical coordinates $\{(r_1, \theta_1, \varphi_1), \dots, (r_K, \theta_K, \varphi_K)\}$, including the distances from the origin, and the elevation and azimuth angles, respectively. From those targets, U out of K with coordinates $\{(r_1, \theta_1, \varphi_1), \dots, (r_U, \theta_U, \varphi_U)\}$ are the DL UEs. Each distance $r_{u,\ell,i,n}$ in (4) and (5) can be calculated as:

$$r_{u,\ell,i,n} = \left((r_{u,\ell} \sin \theta_{u,\ell} \cos \varphi_{u,\ell} + \frac{d_P}{2} + (i-1)d_{\text{RF}})^2 + (r_{u,\ell} \sin \theta_{u,\ell} \sin \varphi_{u,\ell})^2 + (r_{u,\ell} \sin \theta_{u,\ell} - (n-1)d_E)^2 \right)^{\frac{1}{2}}, \quad (7)$$

where $r_{u,\ell}$, $\theta_{u,\ell}$, and $\varphi_{u,\ell}$ represent the distance, and elevation and azimuth angles of each u th UE's ℓ th antenna with respect to the origin, which can be computed as follows:

$$\begin{aligned} \theta_{u,\ell} &= \tan^{-1} \left(\frac{r_u \sin \theta_u + (\ell-1)d_{\text{RF}}}{r_u \cos \theta_u} \right), \\ r_{u,\ell} &= \frac{r_u \cos \theta_u}{\cos \theta_{u,\ell}}, \quad \varphi_{u,\ell} \triangleq \varphi_u. \end{aligned} \quad (8)$$

Note that the elevation angle of each u th UE's ℓ th antenna with respect to the n th element of each i th microstrip is:

$$\theta_{u,\ell,i,n} \triangleq \sin^{-1} \left(\frac{|(n-1)d_E - r_{u,\ell} \cos \theta_{u,\ell}|}{r_{u,\ell,i,n}} \right). \quad (9)$$

The end-to-end channel model including the impinging/reflected components to/from the K targets, when considered as point sources with coordinates $(r_k, \theta_k, \varphi_k) \forall k = 1, \dots, K$, can be expressed as follows:

$$\mathbf{H}_R \triangleq \sum_{k=1}^K \beta_k \mathbf{a}_{RX}(r_k, \theta_k, \varphi_k) \mathbf{a}_{TX}^H(r_k, \theta_k, \varphi_k) \quad (10)$$

with β_k representing the complex-valued reflection coefficient for each k th radar target, whereas, using (5) and the string definition $\text{str} \triangleq \{\text{TX}, \text{RX}\}$, $\mathbf{a}_{\text{str}}(\cdot)$ can be obtained as:

$$[\mathbf{a}_{\text{str}}(r_k, \theta_k, \phi_k)]_{(i-1)N_E+n} \triangleq a_{k,i,n} \exp\left(j\frac{2\pi}{\lambda} r_{k,i,n}\right). \quad (11)$$

In this expression, the elevation angle $\theta_{k,i,n}$ and the distance $r_{k,i,n}$ from the origin for each k th target are needed to compute $a_{k,i,n}$. The former value can be obtained similar to (9), while the latter is given by the following expression:

$$r_{k,i,n} \triangleq \left((r_k \sin \theta_k \cos \phi_k \pm \frac{d_P}{2} \pm (i-1)d_{RF})^2 + (r_k \sin \theta_k \sin \phi_k)^2 + (r_k \cos \theta_k - (n-1)d_E)^2 \right)^{\frac{1}{2}}. \quad (12)$$

In this expression, the positive sign refers to the transmission vector, while the negative sign indicates the reception vector.

B. Received Signal Models

The baseband received signal $\mathbf{y}_u \in \mathbb{C}^{L \times 1}$ at each u th UE can be mathematically expressed as:

$$\mathbf{y}_u \triangleq \mathbf{H}_{DL,u} \mathbf{P}_{TX} \mathbf{W}_{TX} \mathbf{V}_s + \mathbf{n}_u, \quad (13)$$

where $\mathbf{n}_u \sim \mathcal{CN}(\mathbf{0}, \sigma_u^2 \mathbf{I}_L)$ denotes the Additive White Gaussian Noise (AWGN) vector. Similarly, the baseband received signal $\mathbf{y} \in \mathbb{C}^{N_{RF} \times 1}$ at the output of the RX DMA panel of the proposed FD holographic MIMO system is given by:

$$\mathbf{y} \triangleq \mathbf{W}_{RX}^H \mathbf{P}_{RX}^H \mathbf{H}_R \mathbf{P}_{TX} \mathbf{W}_{TX} \mathbf{V}_s + (\mathbf{W}_{RX}^H \mathbf{P}_{RX}^H \mathbf{H}_{SI} \mathbf{P}_{TX} \mathbf{W}_{TX} + \mathbf{D}) \mathbf{V}_s + \mathbf{W}_{RX}^H \mathbf{P}_{RX}^H \mathbf{n}, \quad (14)$$

where $\mathbf{n} \sim \mathcal{CN}(\mathbf{0}, \sigma^2 \mathbf{I}_{N_{RF}})$ denotes the AWGN vector and $\mathbf{H}_{SI} \in \mathbb{C}^{M \times N}$ represents the near-field SI channel, which is defined $\forall i, i' = 1, \dots, N_{RF}$ and $\forall n, n' = 1, \dots, N_E$ as:

$$[\mathbf{H}_{SI}]_{((i-1)N_E+n, (i'-1)N_E+n')} \triangleq \alpha_{i,i',n,n'} \exp\left(j\frac{2\pi}{\lambda} r_{i,i',n,n'}\right),$$

where $\theta_{i,i',n,n'} = \sin^{-1}(|n' - n|d_E/r_{i,i',n,n'})$ and

$$r_{i,i',n,n'} \triangleq \left(\left(\frac{d_P}{2} + (i' - 1)d_{RF} - \left(-\frac{d_P}{2} - (i - 1)d_{RF} \right) \right)^2 + \left((n' - 1)d_E - (n - 1)d_E \right)^2 \right)^{\frac{1}{2}}.$$

It is noted that the term $\tilde{\mathbf{H}}_{SI} \triangleq \mathbf{W}_{RX}^H \mathbf{P}_{RX}^H \mathbf{H}_{SI} \mathbf{P}_{TX} \mathbf{W}_{TX}$ in (14) indicates the residual SI contribution, including the impact of the TX and RX DMAs which will be optimized, together with the digital SI cancellation matrix $\mathbf{D} \in \mathbb{C}^{N_{RF} \times N_{RF}}$, for ISAC in the sequel. Since the considered, in this paper, holographic BF is capable of realizing highly directive beams, we will not use analog SI cancellation units [5].

III. PROPOSED FD-ENABLED ISAC FRAMEWORK

In this section, we design the parameters of the proposed FD holographic MIMO system for near-field ISAC. In particular, we derive the TX/RX DMAs' analog BF matrices, the TX digital BF matrix, and the digital SI cancellation matrix based on a dual objective function including the DL rate and the accuracy of the target parameters' estimation.

A. Near-Field Targets' Parameters Estimation

By using T transmission time slots to construct the reception matrix $\mathbf{Y} \in \mathbb{C}^{N_{RF} \times T}$ using (14), the sample covariance matrix $\mathbf{R} \triangleq \frac{1}{T} \mathbf{Y} \mathbf{Y}^H \in \mathbb{C}^{N_{RF} \times N_{RF}}$ can be computed for estimating the range, and elevation and azimuth angles of the K targets via MULTIPLE Signal Classification. Performing \mathbf{R} 's eigenvalue decomposition, yields $\mathbf{R} = \mathbf{U} \text{diag}\{\eta_1, \eta_2, \dots, \eta_{N_{RF}}\} \mathbf{U}^H$ with $\eta_1 \geq \eta_2 \geq \dots \geq \eta_{N_{RF}}$ being the matrix eigenvalues in descending order and $\mathbf{U} \in \mathbb{C}^{N_{RF} \times N_{RF}}$ including the eigenvectors (η_i associates with eigenvector $\mathbf{u}_i \triangleq [\mathbf{U}]_{:,i}$). In fact, \mathbf{U} can be partitioned as $\mathbf{U} = [\mathbf{U}_s | \mathbf{U}_n]$, where $\mathbf{U}_n \in \mathbb{C}^{N_{RF} \times N_{RF} - K}$ and $\mathbf{U}_s \in \mathbb{C}^{N_{RF} \times K}$ contain the noise- and signal-subspace eigenvectors, respectively. Capitalizing on the orthogonality between the latter subspaces, the 3D MUSIC spectrum can be expressed as a function of the unknown target parameters as follows:

$$\mathcal{M}(r, \theta, \varphi) \triangleq (\mathbf{M}^H \mathbf{U}_K \mathbf{U}_K^H \mathbf{M})^{-K} \prod_{k=1}^{K-1} \mathbf{M}^H \mathbf{U}_k \mathbf{U}_k^H \mathbf{M}, \quad (15)$$

where $\mathbf{U}_K \triangleq [\mathbf{u}_{K+1}, \dots, \mathbf{u}_{N_{RF}}]$ and $\mathbf{M} \triangleq \mathbf{W}_{RX}^H \mathbf{P}_{RX}^H \mathbf{a}_{RX}(r, \theta, \varphi)$. A 3D search on this function's peaks will yield the estimates $(\hat{r}_k, \hat{\theta}_k, \hat{\varphi}_k)$'s for all K targets.

B. FD Holographic MIMO Optimization

Our FD-enabled ISAC design objective is the joint maximization of the Signal-to-Noise-Ratios (SNRs) of the estimation of $(r_k, \theta_k, \varphi_k)$'s for all K targets and of the DL for the U UEs (i.e., the U out of the K targets). In mathematical terms, we focus on the following optimization problem:

$$\begin{aligned} \mathcal{OP} : & \max_{\mathbf{W}_{TX}, \mathbf{W}_{RX}, \mathbf{V}, \mathbf{D}} \hat{\Gamma}_R + \hat{\Gamma}_{DL} \\ \text{s.t.} & \|[\mathbf{W}_{RX}^H \mathbf{P}_{RX}^H \mathbf{H}_{SI} \mathbf{P}_{TX} \mathbf{W}_{TX} \mathbf{V}]_{(i,:)}\|^2 \leq \gamma, \forall i, \\ & \sum_{u=1}^U \|\mathbf{P}_{TX} \mathbf{W}_{TX} \mathbf{V}_u\|^2 \leq P_{\max}, \\ & w_{i,n}^{TX} \in \mathcal{W}, w_{i,n}^{RX} \in \mathcal{W}, \end{aligned}$$

where the SNRs $\hat{\Gamma}_R$ and $\hat{\Gamma}_{DL}$ are given by:

$$\hat{\Gamma}_R \triangleq \left\| \mathbf{W}_{RX}^H \mathbf{P}_{RX}^H \hat{\mathbf{H}}_R \mathbf{P}_{TX} \mathbf{W}_{TX} \mathbf{V} \right\|^2 \hat{\Sigma}^{-1}, \quad (16)$$

$$\hat{\Gamma}_{DL} \triangleq \sum_{u=1}^U \left(\|\hat{\mathbf{H}}_{DL,u} \mathbf{P}_{TX} \mathbf{W}_{TX} \mathbf{V}\|^2 \sigma_u^{-2} \right) \quad (17)$$

with $\hat{\mathbf{H}}_R$ and $\hat{\mathbf{H}}_{DL,u} \forall u$ constructed using $(\hat{r}_k, \hat{\theta}_k, \hat{\varphi}_k)$'s. In the \mathcal{OP} formulation, the first constraint refers to the residual SI threshold γ at the output of each i th microstrip of the RX

DMA. In (16), $\widehat{\Sigma} \triangleq \|\widehat{\mathbf{H}}_{\text{SI}}\mathbf{V}\|^2 + \|\mathbf{P}_{\text{RX}}\mathbf{W}_{\text{RX}}\|^2\sigma^2$ represents the Interference-plus-Noise (IpN) after digital SI cancellation and analog combining at the baseband of the RX DMA.

To solve the non-convex \mathcal{OP} , which has coupling variables, we employ an alternating optimization approach. By utilizing $(\widehat{r}_k, \widehat{\theta}_k, \widehat{\varphi}_k)$'s, the DL channels $\widehat{\mathbf{H}}_{\text{DL},u} \forall u$ are formulated using (4), as well as the composite end-to-end channel $\widehat{\mathbf{H}}_{\text{R}}$ using (10), but without the inclusion of β_k 's, which are unknown. To find the TX/RX DMA analog BF matrices \mathbf{W}_{TX} and \mathbf{W}_{RX} , we first restrict their elements to the set $\mathcal{F} \in e^{j\phi} | \phi \in [-\pi/2, \pi/2]$ (e.g., DFT codebook) having constant amplitude and arbitrary phase values, and then solve the two following optimization problems sequentially via 1D searches:

$$\begin{aligned} \mathcal{OP}1 : \max_{\widetilde{\mathbf{W}}_{\text{TX}}} \|\widehat{\mathbf{H}}_{\text{R}}\widetilde{\mathbf{W}}_{\text{TX}}\|^2, \quad \mathcal{OP}2 : \max_{\widetilde{\mathbf{W}}_{\text{RX}}} \frac{\|\widetilde{\mathbf{W}}_{\text{RX}}\widehat{\mathbf{H}}_{\text{R}}\widetilde{\mathbf{W}}_{\text{TX}}\|^2}{\|\widetilde{\mathbf{W}}_{\text{RX}}\widehat{\mathbf{H}}_{\text{SI}}\widetilde{\mathbf{W}}_{\text{TX}}\|^2} \\ \text{s.t.} \quad \widetilde{w}_{i,n}^{\text{TX}} \in \mathcal{F} \quad \quad \quad \text{s.t.} \quad \widetilde{w}_{i,n}^{\text{RX}} \in \mathcal{F} \end{aligned}$$

Given $\widetilde{\mathbf{W}}_{\text{TX}}$, $\widetilde{\mathbf{W}}_{\text{RX}}$, and compensating for the signal propagation inside the microstrips, the final TX/RX DMA weights can be derived as follows:

$$w_{i,n}^{\text{TX}} \triangleq \frac{J + \widetilde{w}_{i,n}^{\text{TX}} e^{j\rho_{i,n}\beta_i}}{2}, \quad w_{i,n}^{\text{RX}} \triangleq \frac{J + \widetilde{w}_{i,n}^{\text{RX}} e^{j\rho_{i,n}\beta_i}}{2}. \quad (18)$$

Then, we find the multi-user digital BF matrix \mathbf{V} employing block diagonalization, such that it maximizes the SNR of the DL UEs, while minimizing the inter-UE interference and suppressing the residual SI signal at the RX DMA's output below the required threshold. The proposed FD-enabled ISAC design solving \mathcal{OP} is summarized in Algorithm 1. It is noted that, in the algorithmic Step 1, a random feasible \mathbf{W}_{RX} can be used when the ISAC system runs for the first time, or a matrix exploiting any prior knowledge. Then, the targets' parameters estimation can be performed with the optimized \mathbf{W}_{RX} .

IV. NUMERICAL RESULTS AND DISCUSSION

In this section, we numerically evaluate the ISAC performance of the proposed FD holographic MIMO framework, when operating in the sub-THz frequency band and in the near-field regime. We have simulated a scenario including $K = 3$ sensing targets, with $U = 2$ being the UEs each with $L = 2$ antennas, whose direction and range need to be estimated. The proposed FD holographic MIMO node was assumed to deploy TX/RX DMAs, each consisting of $N_{\text{RF}} = \{4, 5, 6\}$ microstrips with each having $N_{\text{E}} = 512$ metamaterials. The microstrips at both DMAs were placed along the x -axis, as shown in Fig. 1, with inter-microstrip distance $d_{\text{RF}} = \lambda/2$. The inter-element distance within each microstrip was set as $d_{\text{E}} = \lambda/5$ and the separation between the TX and RX DMAs was chosen as $d_{\text{pl}} = 2d_{\text{P}} = 0.04$ meters. The central frequency of the proposed ISAC system was 120 GHz covering a bandwidth $B = 150$ KHz. Our Monte Carlo runs for the performance evaluation were designed as follows: we have used $T = 200$ transmission time slots for communications and sensing per UE location, and placed the UE randomly in an environment with a fixed azimuth at 90° , elevation lying in the set $[0^\circ, 90^\circ]$, and a range between 1 and 25 meters (propagation within the

Algorithm 1: FD Holographic MIMO ISAC

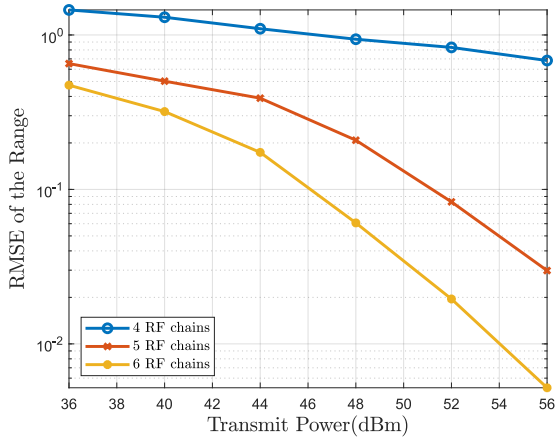
Input: $\mathbf{P}_{\text{TX}}, \mathbf{P}_{\text{RX}}, \mathbf{H}_{\text{SI}}, U$, and P_{max} .

Output: $\mathbf{W}_{\text{TX}}, \mathbf{W}_{\text{RX}}, \mathbf{V}$, and \mathbf{D} .

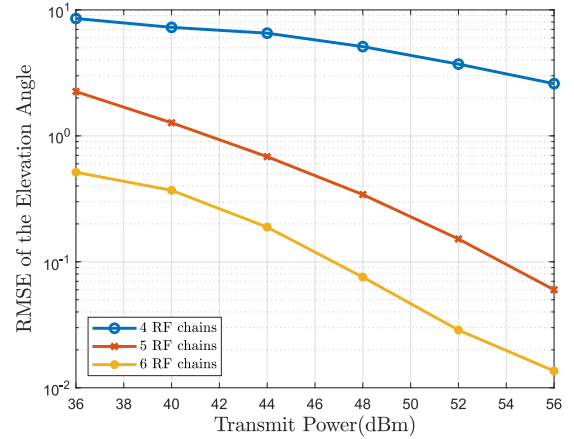
- 1: Obtain $(\widehat{r}_k, \widehat{\theta}_k, \widehat{\varphi}_k) \forall k = 1, \dots, K$ from (15)'s peaks.
 - 2: Set $\widehat{\mathbf{H}}_{\text{R}} = \sum_{k=1}^K \mathbf{a}_{\text{RX}}(\widehat{r}_k, \widehat{\theta}_k, \widehat{\varphi}_k) \mathbf{a}_{\text{TX}}^{\text{H}}(\widehat{r}_k, \widehat{\theta}_k, \widehat{\varphi}_k)$ and construct $\widehat{\mathbf{H}}_{\text{DL},u} \forall u$ using (4).
 - 3: Solve $\mathcal{OP}1$ and $\mathcal{OP}2$ to find $\widetilde{\mathbf{W}}_{\text{TX}}$ and $\widetilde{\mathbf{W}}_{\text{RX}}$.
 - 4: Compute $w_{i,n}^{\text{TX}}$ and $w_{i,n}^{\text{RX}} \forall i, n$ using (18) and obtain \mathbf{W}_{TX} and \mathbf{W}_{RX} .
 - 5: Set $\mathbf{D} = -(\mathbf{W}_{\text{RX}}^{\text{H}} \mathbf{P}_{\text{RX}}^{\text{H}} \mathbf{H}_{\text{SI}} \mathbf{P}_{\text{TX}} \mathbf{W}_{\text{TX}})$ and derive \mathbf{B} as the N_{RF} right-singular vectors of $-\mathbf{D}$.
 - 6: **if** $U = 1$ **then**
 - 7: Set $\mathbf{G} = \sqrt{P_{\text{max}}}\mathbf{E}$ with \mathbf{E} having the right-singular vectors of $\mathbf{H}_{\text{eff},1} = \widehat{\mathbf{H}}_{\text{DL},1} \mathbf{P}_{\text{TX}} \mathbf{W}_{\text{TX}} \mathbf{B}$.
 - 8: **if** $\|[\mathbf{W}_{\text{RX}}^{\text{H}} \mathbf{P}_{\text{RX}}^{\text{H}} \mathbf{H}_{\text{SI}} \mathbf{P}_{\text{TX}} \mathbf{W}_{\text{TX}} \mathbf{B} \mathbf{G}]_{(i,:)}\|^2 \leq \gamma, \forall i$ **then**
 - 9: Output $\mathbf{V} = \mathbf{B} \mathbf{G}$ and stop the algorithm.
 - 10: **else**
 - 11: Output that the FD holographic MIMO settings do not meet the residual SI constraints.
 - 12: **end if**
 - 13: **end if**
 - 14: **for** $u = 1, 2, \dots, U$ **do**
 - 15: **for** $\alpha = N_{\text{RF}}, N_{\text{RF}} - 1, \dots, L$ **do**
 - 16: Set $\mathbf{F} = [\mathbf{B}]_{(:, N_{\text{RF}} - \alpha + 1 : N_{\text{RF}})}$ and $\mathbf{H}_{\text{eff},u} = \widehat{\mathbf{H}}_{\text{DL},u} \mathbf{P}_{\text{TX}} \mathbf{W}_{\text{TX}} \mathbf{F}$.
 - 17: Set $\mathbf{K}_u \in \mathbb{C}^{N_{\text{RF}} \times L}$ as the null space of the effective DL channel with the u th UE removed: $\widetilde{\mathbf{H}}_{\text{eff},u} \triangleq [\mathbf{H}_{\text{eff},1}, \dots, \mathbf{H}_{\text{eff},u-1}, \mathbf{H}_{\text{eff},u+1}, \dots, \mathbf{H}_{\text{eff},U}]$.
 - 18: Set $\widetilde{\mathbf{E}}_u \in \mathbb{C}^{N_{\text{RF}} \times (L-1)}$ as the right-singular vectors of \mathbf{K}_u .
 - 19: Set \mathbf{E}_u as the right singular vectors of $\mathbf{H}_{\text{eff},u} \widetilde{\mathbf{E}}_u$.
 - 20: Set $\mathbf{G}_u = \sqrt{P_{\text{max}}/U} \mathbf{E}_u \mathbf{E}_u$ as the optimum block-diagonalized precoder for the u th UE.
 - 21: **end for**
 - 22: Construct digital precoder $\mathbf{G} = [\mathbf{G}_1, \dots, \mathbf{G}_U]$.
 - 23: **if** $\|[\mathbf{W}_{\text{RX}}^{\text{H}} \mathbf{P}_{\text{RX}}^{\text{H}} \mathbf{H}_{\text{SI}} \mathbf{P}_{\text{TX}} \mathbf{W}_{\text{TX}} \mathbf{F} \mathbf{G}]_{(i,:)}\|^2 \leq \gamma, \forall i$ **then**
 - 24: Output $\mathbf{V} = \mathbf{F} \mathbf{G}$ and stop the algorithm.
 - 25: **else**
 - 26: Output that the FD holographic MIMO settings do not meet the residual SI constraints.
 - 27: **end if**
 - 28: **end for**
-

Fresnel region). Finally, the noise variances σ^2 and σ_1^2 in dB were set to $-174 + 10 \log_{10}(B)$, β_1 appearing in (10) was chosen randomly with unit amplitude, and we have used a 10-bit beam codebook \mathcal{F} for both the TX/RX DMA analog BF matrices \mathbf{W}_{TX} and \mathbf{W}_{RX} in $\mathcal{OP}1$.

In Figs. 2 and 3, simulation results for the proposed FD-enabled ISAC scheme detailed in Algorithm 1 are illustrated for different total transmit power levels P_{max} in dBm, which are typical for sub-THz wireless communications. In particular,



(a) Range estimation.



(b) Estimation of the elevation angle.

Fig. 2: Average sensing estimation performance for $U = 2$ UEs, each with $L = 2$ antenna elements, versus the transmit power P_{\max} in dBm, considering an FD holographic MIMO node with $N_{\text{RF}} = \{4, 5, 6\}$ TX/RX microstrips each with $N_E = 512$ metamaterials.

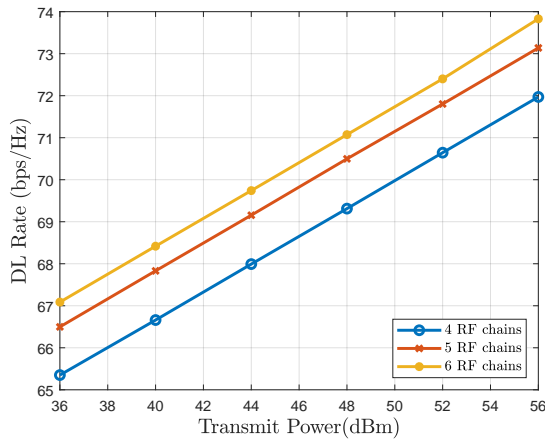


Fig. 3: Achievable DL rate versus the transmit power P_{\max} in dBm for the parameters' setting in Fig. 2.

Figs. 2a and 2b demonstrate the Root Mean Square Error (RMSE) of the estimations for the range and the elevation angle, respectively, whereas Fig. 3 depicts the achievable DL rate performance in bps/Hz. As expected, all performance metrics improve with increasing SNR values, and it is showcased that, increasing the number of microstrips (consequently, the number of TX/RX RF chains) improves both estimation performance and the DL rate. The latter is reasonable since more spatial sampling improves the target parameter estimation, which in turn, improves DL channel estimation. This, in conjunction with, the larger BF gain, results in rate boosting.

V. CONCLUSION

In this paper, we presented an FD holographic MIMO ISAC system, operating in THz frequencies and in the near-field regime, capable to offer simultaneous multi-user DL communication and sensing of targets being randomly distributed within its coverage area. A novel optimization framework for the joint design of the TX/RX DMAs' analog BF matrices, the TX digital BF matrix, and the digital SI cancellation matrix was

devised. Our numerical results showcased the ISAC potential of the proposed scheme for various system parameters.

REFERENCES

- [1] F. Liu *et al.*, "Integrated sensing and communications: Towards dual-functional wireless networks for 6G and beyond," *IEEE J. Sel. Areas Commun.*, 2022.
- [2] K. V. Mishra *et al.*, "Toward millimeter-wave joint radar communications: A signal processing perspective," *IEEE Signal Process. Mag.*, vol. 36, no. 5, pp. 100–114, Sep. 2019.
- [3] A. Sabharwal *et al.*, "In-band full-duplex wireless: Challenges and opportunities," *IEEE J. Sel. Areas Commun.*, vol. 32, no. 9, pp. 1637–1652, Sep. 2014.
- [4] G. C. Alexandropoulos and M. Duarte, "Joint design of multi-tap analog cancellation and digital beamforming for reduced complexity full duplex MIMO systems," in *Proc. IEEE ICC*, Paris, France, May 2017.
- [5] G. C. Alexandropoulos *et al.*, "Full duplex massive MIMO architectures: Recent advances, applications, and future directions," *IEEE Veh. Technol. Mag.*, vol. 17, no. 4, pp. 83–91, Dec. 2022.
- [6] I. P. Roberts *et al.*, "Equipping millimeter-wave full-duplex with analog self-interference cancellation," in *Proc. IEEE ICC*, Ireland, Jun. 2020.
- [7] G. C. Alexandropoulos *et al.*, "Full duplex hybrid A/D beamforming with reduced complexity multi-tap analog cancellation," in *Proc. IEEE SPAWC*, Atlanta, USA, May 2020.
- [8] C. B. Barneto *et al.*, "Full-duplex OFDM radar with LTE and 5G NR waveforms: Challenges, solutions, and measurements," *IEEE Trans. Microw. Theory Techn.*, vol. 67, no. 10, pp. 4042–4054, Aug. 2019.
- [9] S. D. Liyanaarachchi *et al.*, "Optimized waveforms for 5G–6G communication with sensing: Theory, simulations and experiments," *IEEE Trans. Wireless Commun.*, Jun. 2021.
- [10] C. B. Barneto *et al.*, "Beamforming and waveform optimization for OFDM-based joint communications and sensing at mm-waves," in *Proc. IEEE ASILOMAR*, Pacific Grove, USA, Nov. 2020, pp. 895–899.
- [11] M. A. Islam *et al.*, "Integrated sensing and communication with millimeter wave full duplex hybrid beamforming," in *Proc. IEEE ICC*, Seoul, South Korea, May. 2022.
- [12] —, "Simultaneous multi-user MIMO communications and multi-target tracking with full duplex radios," in *Proc. IEEE GLOBECOM*, Rio de Janeiro, Brazil, Dec. 2022.
- [13] N. Shlezinger *et al.*, "Dynamic metasurface antennas for 6G extreme massive MIMO communications," *IEEE Wireless Commun.*, vol. 28, no. 2, pp. 106–113, Apr. 2021.
- [14] T. Gong *et al.*, "Holographic MIMO communications: Theoretical foundations, enabling technologies, and future directions," *arXiv preprint arXiv:2212.01257*, 2022.
- [15] J. Xu *et al.*, "Near-field wideband extremely large-scale MIMO transmission with holographic metasurface antennas," *arXiv preprint arXiv:2205.02533*, 2022.